17th World Conference on Earthquake Engineering, 17WCEE
Sendai, Japan - September 13th to 18th 2020

SEISMIC ANALYSIS OF A TWO-SPAN MASONRY ARCH BRIDGE

P. Clemente[(1)] and F. Saitta[(2)]

[(1)] *Research Director, ENEA Casaccia Research Centre, paolo.clemente@enea.it*
[(2)] *Researcher, ENEA Casaccia Research Centre, fernando.saitta@enea.it*

Abstract

Quick evaluation of seismic safety in existing bridge structures needs reliable and simple methods of analysis, at least for preliminary approaches, reserving more complex methods such as those based on finite elements to deeper investigations. Among existing bridges stone and masonry arches were widely built in the past and are still in service under more and more increasing traffic loads.

The mechanism method is certainly a good candidate to satisfy the requirements of simplicity and rapidity. The main hypothesis is that stone arches fail by forming pin joints, as demonstrated by old but also by recent experimental studies. Furthermore, the assumption of masonry with no tensile strength and infinite compressive strength was done in the starting applications of the method. This last hypothesis was removed in previous papers, by assuming a rigid-perfect plastic behavior in compression. The load factor and the corresponding collapse mechanism are found by using an iteration procedure. The model has been applied also for the analysis of two-span arch bridges under vertical loads, so that the collapse mechanism involves plastic hinges in the two arches and the pier. In this paper the two-span arch under horizontal seismic load is considered, assuming static forces according to a uniform distribution of horizontal accelerations.

Keywords: Multi-span arch bridges, Mechanism method, Masonry arches, Limit behavior, Seismic analysis.

1. Introduction

If compared with the other numerical techniques, the mechanism method has the advantage of simplicity, clarity of the solution, and speed of the analysis. Therefore, it can be very useful in expeditious approaches to safety assessment. On the basis of the limit analysis developed in the eightieth century, Kooharian [1] and then Heyman [2, 3] established the principles for the application of the limit analysis to masonry structures. The mechanism method has been extensively applied for the stability assessment of masonry arch bridges, assuming the hypotheses of no tensile strength but infinite strength in compression for the material. A wide numerical investigation was carried out by Clemente et al. [4] on the influence of the geometrical and loading parameters on the limit behavior of a single span arch bridge subject to dead plus vertical live loads.
The mechanism model allowed studying also the limit behavior under dead plus seismic loads with different hypotheses about the interaction between the fill and the ring [5]. The complex dynamic behavior of a single arch subject to base motion was also studied [6, 7]. The analysis carried out in [7], in detail, referred to the first half cycle of vibration of an arch under sinusoidal base acceleration and focused the attention on the importance of frequency content and amplitude of the input and the initial conditions.
While the hypothesis of no tension strength is almost true for masonry, that of infinite compression strength could be quite far from the reality. Several authors considered the case of finite compression strength. Among these, Crisfield and Packham [8] who developed a numerical procedure to evaluate the collapse load for masonry arch bridges. The load spreading in the fill was considered as well as the lateral earth resistance. The importance of considering a finite strenght in compression was emphasized especially for reinforced masonry arch bridges [9, 10]. Clemente et al. [11] analyzed the effect of the reduction of the effective design thickness on the limit behavior. The reduction was correlated to the material actual strength and the results gave a measure of the obvious reduction of the load factor but pointed out also a negligible influence on the hinge locations.
More recently, a rigid-perfect plastic model with finite compression strength for the masonry has been proposed for a single span arch bridge [12]. The new model was already tested also with reference to the limit behavior under seismic actions [13, 14], using different hypotheses about the interaction between the fill and the ring.
Little interest has been devoted in the past to the limit analysis of multi-span masonry arch bridges. An analysis of a two-span arch bridge under vertical static loads is in [15]; the Heyman's hypothesis of infinite compression strength of masonry was assumed. Using the same model, a comprehensive analysis is also in [11], where the limit behavior of a two-span masonry arch bridge was analyzed in detail under dead and travelling loads. The approach based on limit analysis for multi-span arch bridges is questioned in [16], pointing out that often masonry compression strength can be reached before the collapse mechanism is activated. The already mentioned rigid-perfect plastic model with finite compression strength for the material has been used also for a two span masonry arch bridge under dead and travelling loads [17].
In this paper the limit analysis of a two-span masonry arch bridge, with equal spans, under horizontal seismic actions is carried out assuming a rigid-perfect plastic model for masonry with finite strength in compression. The fill is considered for its weigh and inertial load acting on the arch ring; its contribution in the structural resistance is not considered.

2. Statics and kinematic of collapse mechanism

2.1 The plastic hinge

In the hypothesis of no tensile strenght and rigid-perfect plastic behavior of masonry in compression, the effective cross-section at hinges is uniformely compressed with the tension equal to f_m, and the relative rotation points are at the internal starting points of the stress diagram. As a consequence, the compression force at hinges does not pass through the rotation point, but at half depth of the yielded zone (Fig. 1). The limit domain is also represented in Fig 1 in terms of non-dimensional eccentricity $\hat{e}$ and axial force $\hat{N}$.

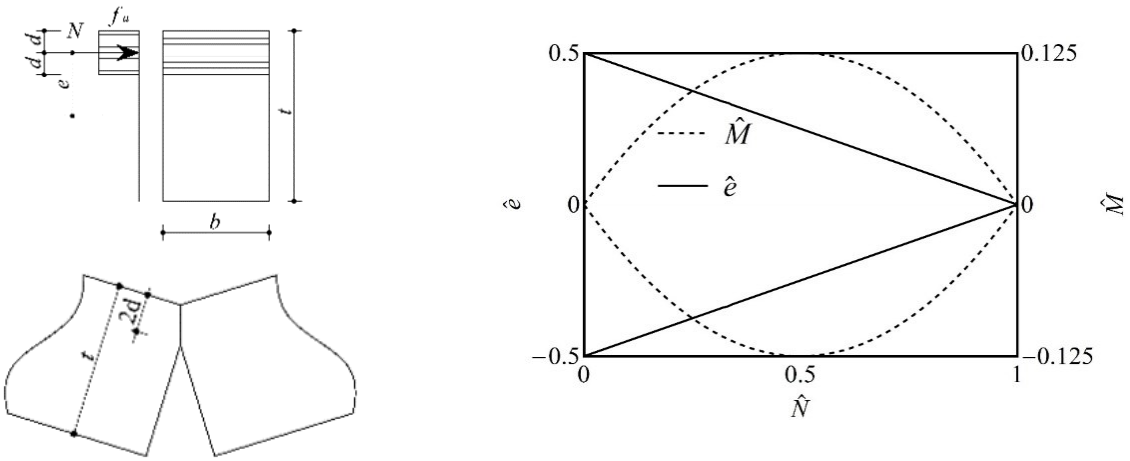

Fig. 1 – Stress on the cross section at hinge and kinematic behaviour in the hypotheses of finite compression strength (left) and limit domain

2.1 Kinematic of the mechanism

Depending on geometry, materials and load, the collapse mechanism of a two-span arch bridge under a generic loading could involve a single arch only or be a global mechanism, whihc involves both the spans and the pier. The global collapse mechanism of the system is characterized by at least seven hinges deployed as in Fig. 2. According to limit analysis, the collapse mechanism and the corresponding load factor can be found by using an iteration procedure based on the kinematic and static theorems. For a given admissible mechanism, the diagram of virtual vertical displacements of the two arch spans and pier can be plotted (Fig. 2).

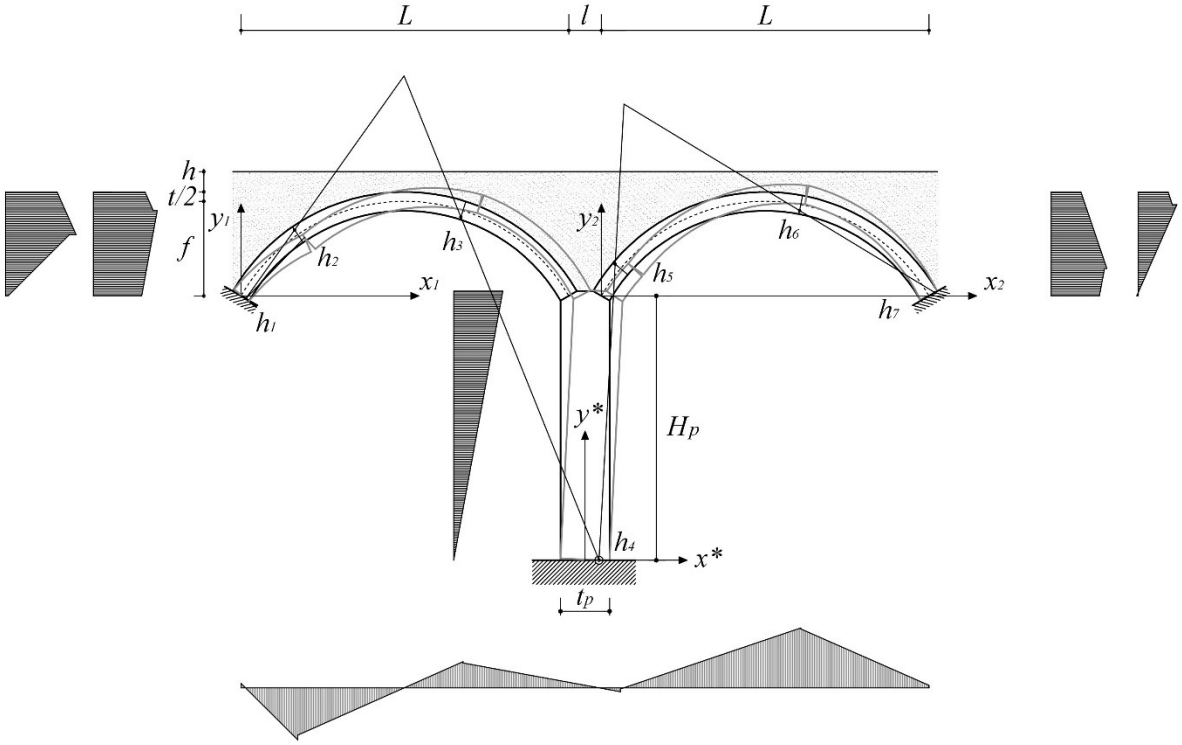

Fig. 2 – Two-span arch bridge and collapse mechanism

For each arch (i = 1, 2), the distributed dead load of the ring is given as follows:

$$w(x_i) = \gamma_w b\, t(x_i)/\cos\alpha(x_i) \tag{1}$$

whereas the backfill dead is:

$$w_b(x_i) = \gamma_b b[h + f + t(L/2)/2 - y(x_i) - t(x_i)/2\cos\alpha(x_i)] \tag{2}$$

In the previous formulas, b is the width of the arches, $\alpha(x_i)$ is the angle between the tangent to the arch centre line at x_i and the horizontal axis, γ_w is the weight per unit volume of the ring material, γ_b that of the backfill. The other quantities are shown in Fig. 2.

The self-weight of the pier can be expressed as (b_p = width of the pier):

$$w_p(y^*) = \gamma_w b_p t_p(y^*) \tag{3}$$

If the he following non-dimensional quantities are introduced:

$$\hat{x}_i = \frac{x_i}{L}; \quad \hat{h} = \frac{h}{L}; \quad \hat{f} = \frac{f}{L}; \quad \hat{t}(\hat{x}_i) = \frac{t(\hat{x}_i L)}{L}; \quad \hat{y}(\hat{x}_i) = \frac{y(\hat{x}_i L)}{L}; \quad \hat{t}_p(\hat{y}^*) = t_p(\hat{y}^* L)/L \tag{4}$$

from Eqs. (1)-(3):

$$\hat{w}(\hat{x}_i) = w(x_i)/\gamma_w bL; \quad \hat{w}_b(\hat{x}_i) = w_b(x_i)/\gamma_w bL; \quad \hat{w}_p(\hat{y}^*) = w_p(y^*)/\gamma_w bL \tag{5}$$

The work associated to ring, backfill and pier self-loads is expressed in non-dimensional way as follows:

$$L_w = \gamma_w bL^3 \left\{\sum_{i=1}^{2} \int_0^1 \left[\hat{w}_{w,i}(\hat{x}_i)\hat{\eta}(\hat{x}_i) + \hat{w}_{b,i}(\hat{x}_i)\hat{\eta}(\hat{x}_i)\right] d\hat{x}_i + \hat{\eta}^* \left[\hat{W}_{b,p} + \int_0^{H_p/L} \hat{w}_p(\hat{y}^*) d\hat{y}^*\right]\right\} \tag{6}$$

where $\hat{W}_{b,p}$ is the load given by the portion of the fill over the pier.

In the previous equation, the weight of the pier per unit length is deduced by some manipulation:

$$\hat{w}_p(\hat{y}^*) = w_p(\hat{y}^* L)/\gamma_w bL = \tilde{b}\hat{t}_p(\hat{y}^* L) \tag{7}$$

with $\tilde{b} = b_p/b$.

The horizontal load depends on the model assumed for the structure-backfill interaction. The arch is subject to the horizontal inertial loads due to the mass of the ring. The horizontal inertial actions due to the mass of the backfill, present from the abutment to the arch profile, is considered only on half of the arch, while the backfill is supposed to tend to separate from the arch at the other half. If a_g is the horizontal acceleration and we assume the hypothesis of rigid behavior of the structure before the mechanism activation, the two half spans and the pier are loaded as follows:

$$p_{h,1}(x_1) = \left[w_w(x_1) + \gamma_b \tan\alpha \left(x_1 - \frac{t}{2sin\alpha}\right)\right] a_g/g \tag{8}$$

$$p_{h,2}(x_2) = \left[w_w(x_2) + \gamma_b \tan\alpha \left(2x_2 + l - \frac{t}{sin\alpha}\right)\right] a_g/g \tag{9}$$

$$p_{h,p}(y^*) = w_p(y^*) a_g/g \tag{10}$$

The virtual work done by an external horizontal inertial load can be expressed as follows:

$$L_p = \int_{x_{1,0}}^{L/2} p_{h,1}(x_1)\xi(x_1)\, dx_1 + \int_{x_{2,0}}^{L/2} p_{h,2}(x_2)\xi(x_2)\, dx_2 + \int_{x_{4,0}}^{Hp} p_{h,p}(y^*)\xi(y^*)\, dy^* \tag{11}$$

where $x_{i,0}$ are the starting points of the load $p_{h,i}$ and ξ the horizontal virtual displacement. Finally, the internal work at the seven hinges is:

$$L_i = 2\sum_{i=1}^{7} bf_u d_i^2 \Delta\varphi_i = 2\gamma_w bL^3 \sum_{i=1}^{7} \sigma \hat{d}_i^2 \Delta\varphi_i \tag{12}$$

Therefore, the collapse acceleration value, i.e., the kinematic load multiplier, associated to the chosen collapse mechanism, is calculated as follows:

$$\hat{a}_g = (L_i - L_w)/L_p \tag{13}$$

where $\hat{a}_g = a_g/g$.

2.2 Equilibrium conditions

Once the load factor corresponding to the assigned collapse mechanism is found, one can calculate the variable load and the external forces, by means of six equilibrium equations:

- Horizontal equilibrium of the whole structure:

$$\hat{H}^{(1)} + \hat{H}^{(12)} + \hat{H}^{(2)} + \lambda\left[\int_{\hat{x}_{h1}}^{1} \hat{p}_{h,1}(\hat{x}_1)d\hat{x}_1 + \int_{0}^{\hat{x}_{h7}} \hat{p}_{h,2}(\hat{x}_2)\, d\hat{x}_2 + \int_{\hat{x}_{h4}}^{H_p/L} \hat{p}_{h,p}(\hat{y}^*)d\hat{y}^*\right] = 0 \tag{14}$$

- Vertical equilibrium of the whole structure:

$$\hat{V}^{(1)} + \hat{V}^{(12)} + \hat{V}^{(2)} - \int_{\hat{x}_{h1}}^{1}\left[\hat{w}_{w,1}(\hat{x}_1) + \hat{w}_{b,1}(\hat{x}_1)\right] d\hat{x}_1 - \int_{0}^{\hat{x}_{h7}}\left[\hat{w}_{w,2}(\hat{x}_2) + \hat{w}_{b,2}(\hat{x}_2)\right] d\hat{x}_2 - \int_{\hat{x}_{h4}}^{H_p/L} \hat{w}_p(\hat{y}^*)d\hat{y}^* - \hat{W}_{b,p} = 0 \tag{15}$$

- Rotation by hinge h_1:

$$\begin{aligned}\hat{H}^{(12)} r_{14,y} + \hat{H}^{(2)} r_{17,y} - \hat{V}^{(12)} r_{14,x} - \hat{V}^{(2)} r_{17,x} &+ \int_{\hat{x}_{h1}}^{1}\left[\hat{w}_{w,1}(\hat{x}_1) + \hat{w}_{b,1}(\hat{x}_1)\right](\hat{x}_1 - \hat{x}_{h1})d\hat{x}_1 \\ &+ \int_{0}^{\hat{x}_{h7}}\left[\hat{w}_{w,2}(\hat{x}_2) + \hat{w}_{b,2}(\hat{x}_2)\right]\left(\hat{x}_2 + 1 + \frac{l}{L} - \hat{x}_{h1}\right)d\hat{x}_2 + \left(1 + \frac{l}{2L} - \hat{x}_{h1}\right)\left[\hat{W}_{b,p} + \int_{\hat{x}_{h4}}^{\frac{H_p}{L}} \hat{w}_p(\hat{y}^*)d\hat{y}^*\right] + \\ + \int_{\hat{x}_{h1}}^{1/2} \lambda\, \hat{p}_{h,1}(\hat{x}_1)[\hat{y}(\hat{x}_1) - \hat{y}(\hat{x}_{h1})]d\hat{x}_1 + \int_{0}^{1/2} \hat{p}_{h,2}(\hat{x}_2)[\hat{y}(\hat{x}_2) - \hat{y}(\hat{x}_{h1})]\, d\hat{x}_2 - \int_{\hat{y}_{h4}(}^{\hat{H}_p} \hat{p}_{h,p}(\hat{y}^*)\left[\hat{H}_p - \hat{y}^* + \hat{y}_{h4} - \hat{y}_{1,h1}\right]d\hat{y}^* = 0\end{aligned} \tag{16}$$

- Rotation by hinge h_1 of the portion between h_1 and h_3:

$$-\hat{H}^{(1)} r_{13,y} + \hat{V}^{(1)} r_{13,x} - \int_{\hat{x}_{h1}}^{\hat{x}_{h3}}\left[\hat{w}_{w,1}(\hat{x}_1) + \hat{w}_{b,1}(\hat{x}_1)\right](\hat{x}_{h3} - \hat{x}_1)d\hat{x}_1 - \int_{\hat{x}_{h1}}^{1/2} \lambda\, \hat{p}_{h,1}(\hat{x}_1)[\hat{y}(\hat{x}_{h3}) - \hat{y}(\hat{x}_1)]d\hat{x}_1 = 0 \tag{17}$$

- Rotation by h_5 of the portion between h_5 and h_7:

$$\hat{H}^{(2)} r_{57,y} - \hat{V}^{(2)} r_{57,x} + \int_{\hat{x}_{h5}}^{\hat{x}_{h7}}\left[\hat{w}_{w,2}(\hat{x}_2) + \hat{w}_{b,2}(\hat{x}_2)\right](\hat{x}_2 - \hat{x}_{h5})d\hat{x}_2 - \int_{\hat{x}_{h5}}^{1/2} \lambda\, \hat{p}_{h,2}(\hat{x}_2)[\hat{y}(\hat{x}_{h5}) - \hat{y}(\hat{x}_2)]d\hat{x}_2 = 0 \tag{18}$$

- Rotation by h_2 of the portion between h_2 and h_7:

$$\hat{H}^{(12)}r_{24,y} + \hat{H}^{(2)}r_{27,y} - \hat{V}^{(12)}r_{24,x} - \hat{V}^{(2)}r_{27,x} + \int_{\hat{x}_{h2}}^{1}\left[\hat{w}_{w,1}(\hat{x}_1) + \hat{w}_{b,1}(\hat{x}_1)\right](\hat{x}_1 - \hat{x}_{h2})d\hat{x}_1 + \int_{0}^{\hat{x}_{h7}}\left[\hat{w}_{w,2}(\hat{x}_2) + \hat{w}_{b,2}(\hat{x}_2)\right](\hat{x}_2 + 1 + l/L - \hat{x}_{h2})d\hat{x}_2 + (1 + l/2L - \hat{x}_{h2})\left[\hat{W}_{b,p} + \int_{\hat{x}_{h4}}^{H_p/L}\hat{w}_p(\hat{y}^*)d\hat{y}^*\right] + \int_{\hat{x}_{h2}}^{1/2}\lambda\,\hat{p}_{h,1}(\hat{x}_1)[\hat{y}(\hat{x}_1) - \hat{y}(\hat{x}_{h2})]d\hat{x}_1 + \int_{0}^{1/2}\hat{p}_{h,2}(\hat{x}_2)[\hat{y}(\hat{x}_2) - \hat{y}(\hat{x}_{h2})]\,d\hat{x}_2 - \int_{\hat{y}_{h4}(}^{\hat{H}_p}\hat{p}_{h,p}(\hat{y}^*)\left[\hat{H}_p - \hat{y}^* + \hat{y}_{h4} - \hat{y}_{1,h2}\right]d\hat{y}^* = 0 \quad (19)$$

In the previous equations, the superscript *(i)* of forces $\hat{H}$ and $\hat{V}$ identifies the horizontal and vertical forces on arch *(1)* or *(2)*, and on pier *(12)*. Furthermore, $r_{ij,x}$ and $r_{ij,y}$ are the horizontal and vertical distance, respectively, between the points of applications of forces at hinges h_i and h_j.

Limit analysis under horizontal forces

As well known, the actual load factor is the only one that is contemporarily a kinematically and statically admissible factor. The solution is searched iteratively assuming a starting set of hinge positions. Then, the corresponding collapse acceleration value is calculated using the principle of virtual works and then the reaction forces can be found. The couples $\hat{e}$, $\hat{N}$ are then evaluated. If the corresponding points are always internal to the limit domains of cross-sections of the arch and pier, the found load factor is also a statically admissible load factor. If it is not, the hinges are moved to the sections where the exceedances are maximum. The iteration procedure will be stopped when the kinematically admissible load factor is also a statically admissible load factor.

As an example, let consider a two-span arch bridge with the following geometrical characteristics and γ:

$$\hat{f} = 0.25; \quad \hat{h} = 0.0; \quad \hat{t} = 0.06; \quad \hat{t}_p = 0.1; \quad \hat{H}_p = 0.6; \quad \gamma = 0.5 \quad (20)$$

In the hypothesis of rigid behavior up to the onset of the collapse mechanism, the bridge is subject to a uniform horizontal acceleration (Fig. 3). The collapse acceleration value depends on the non-dimensional stress parameter $\sigma = f_u/\gamma_w L$ (where f_u= ultimate stress of masonry and γ_w= weight for unit volume of masonry) [12]. For $\sigma = 7$ the collapse acceleration is $\hat{a}_g = 0.29$ whereas in the case of infinite strength it is $\hat{a}_g = 0.35$. The corresponding line of thrust on the point of collapse is shown in Fig. 4. In the same Fig. 4, the virtual vertical displacement diagram for the two spans are plotted, for an arbitrary rotation at the hinge h_1. The horizontal virtual displacements of the two spans and the pier are also plotted as well as the polygon of forces at the intersection of pier and rings for the considered case.

Figs. 5a and 5b show the values of the non-dimensional eccentricity versus the axial force, for the arches and the pier. Two values of parameter σ are considered: σ = 5 in Fig. 5a and σ = 7 in Fig. 5b. The limit domain is represented by red lines. Magenta curve is related with the thrust along the pier, black curve is related with the first arch and blue curve with the second arch. Points on the limit domain are related to hinges.

The influence of the parameter σ on the collapse acceleration is shown in Fig. 6. When σ increases the collapse acceleration value approaches to that one obtained using the Heyman's model (Fig. 6). For σ = 5, which is of practical interest in most existing bridges, the collapse acceleration reduces of more than 20% with respect to the Hayman's value.

Finally, Fig. 7 shows the depth of the yielded sections at the seven hinges. It reduces more and more with the increasing of σ.

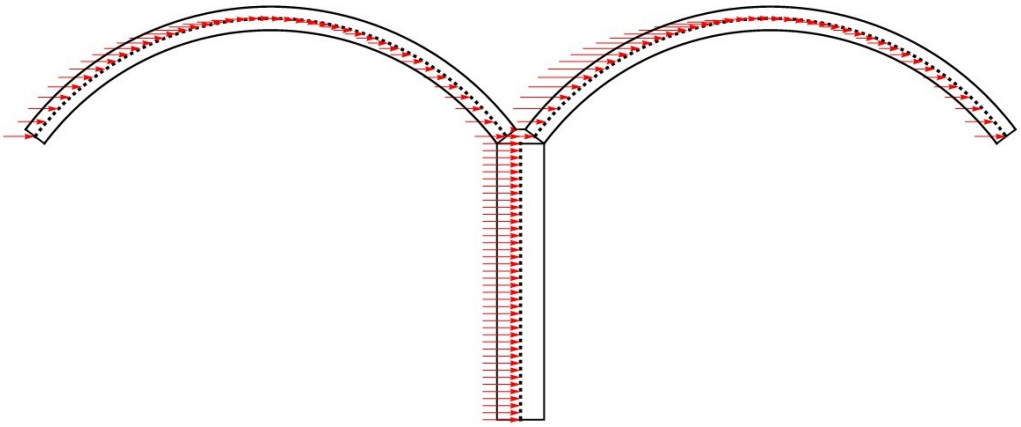

Fig. 3 – Horizontal load distribution

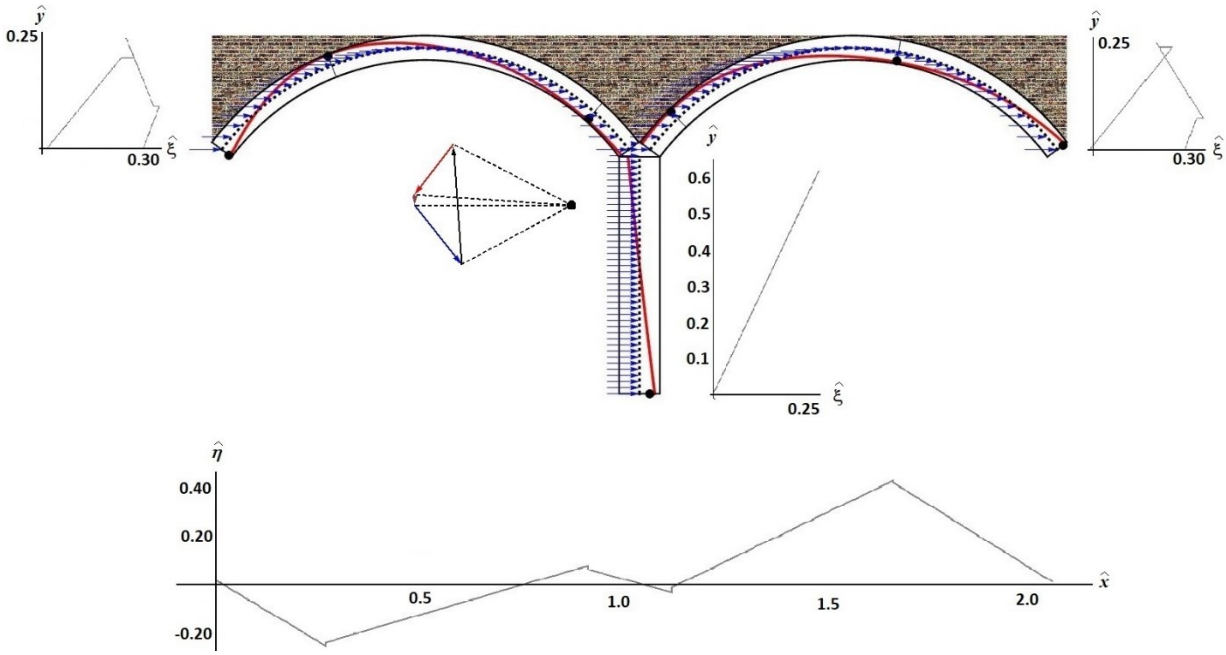

Fig. 4. Line of thrust, virtual displacement diagrams and equilibrium at intersection of rings and pier.

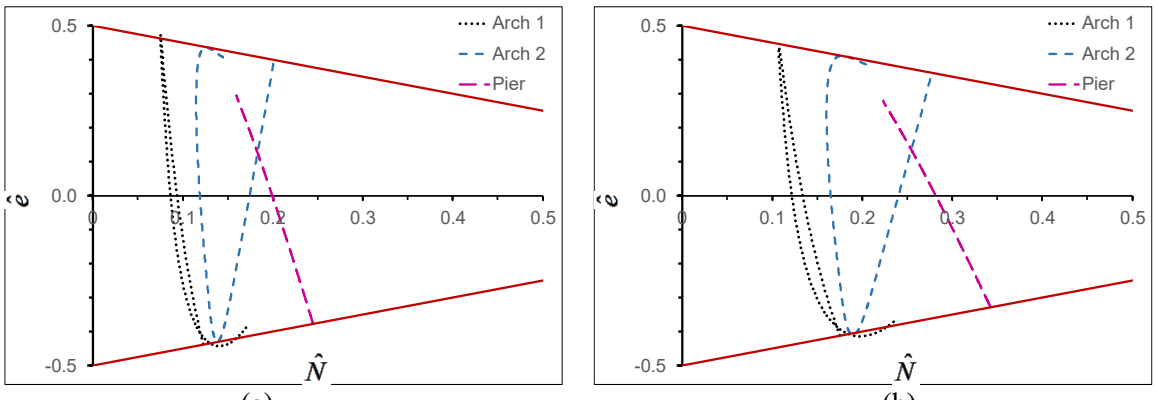

(a) (b)

Fig. 5. Eccentricity versus axial force in the two span and pier for (a) σ = 5 and (b) σ=7.

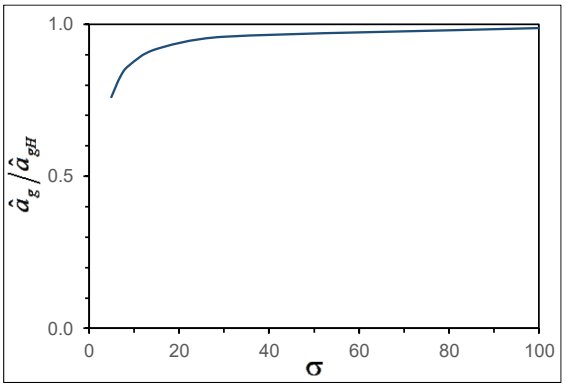

Fig. 6. Collapse acceleration versus material parameter σ.

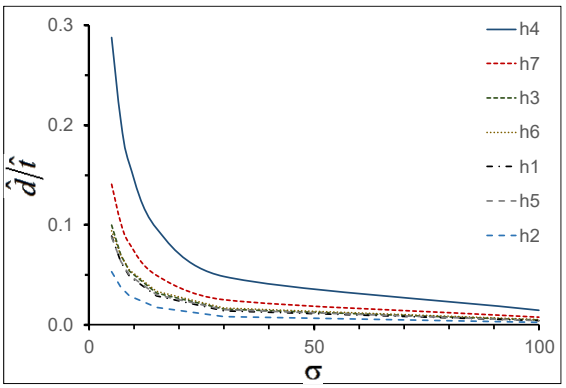

Fig. 7. Yielded depth at hinges versus σ.

4. Conclusions

The limit analysis has been applied for the evaluation of safety of masonry two-span bridges under seismic loadings. The proposed method assumes no tensile strength and a finite resistance of the material in compression. Even if it belongs to the field of simplified methods and some contributions are not considered, the speed in the analysis and the evaluation of general solutions is certainly of practical interest. A seven hinge mechanism for non-symmetric loads is considered and equilibrium equations have been written, finding the collapse acceleration. Results are shown for a selected case, varying the material strength, with reference to non-dimensional parameters. With respect to the case of infinite strength in compression of the material, the method highlights significant differences in the range of practical interest.

Acknowledgements

This paper has been prepared in the framework of the European project ARCH – Advancing Resilience of historic areas against Climate-related and other Hazards. This project has received funding from the European Union's Horizon 2020 research and innovation programme under grant agreement no. 820999. The sole responsibility for the content of this publication lies with the authors. It does not necessarily represent the opinion of the European Union. Neither the EASME nor the European Commission are responsible for any use that may be made of the information contained therein.

6. References

[1] Kooharian A (1952): Limit analysis of voussoir (segmental) and concrete arches. *J. Am. Concr. Inst.*, **24**(4), 317-328.

[2] Heyman J (1966): The stone skeleton. *Int. J. Solids Struct*. **2**(2), 249-279 (1966).

[3] Heyman J (1969): The safety of masonry arches. *Int. J. Mech. Sci.*, **11**(4), 363-385.

[4] Clemente P, Occhiuzzi A, Raithel A (1995): Limit behavior of stone arch bridges. *J. Struct. Eng*., **121**(7), 1045-1050, doi: 10.1061/(ASCE)0733-9445(1995)121:7(1045).

[5] Clemente P. and Raithel A. (1998): The mechanism model in the seismic check of stone arches. In: Sinopoli A. (ed) Arch Bridges, 123-129, Balkema, Rotterdam.

[6] Oppenheim I.J. (1992): The Masonry Arch as a Four-Link Mechanism under Base Motion. *Earthquake Engineering and Structural Dynamics*, **21**(11), 1005-1017, https://doi.org/10.1002/eqe.4290211105.

[7] Clemente P. (1998): Introduction to dynamics of stone arches. *Earthquake Engineering and Structural Dynamics*, **27**(5), 513-522, John Wiley & Sons, https://doi.org/10.1002/(SICI)1096-9845(199805)27:5<513::AID-EQE740>3.0.CO;2-O.

[8] Crisfield M.A. and Packham A.J. (1987): A mechanism program for computing the strength of masonry arch bridges. *Research Rep. No. 124*, Transport and Road Research Laboratory, Crowthorne, Berkshire.

[9] Buffarini, G., Clemente, P., De Felice, G. (2006): Retrofitting of masonry arch bridges with FRP. In: P.B. Lourenço, P. Roca, C. Modena, S. Agrawal (eds.), SAHC06. Macmillian India Ltd, Delhi.

[10] De Felice G., Carbone I., Clemente P. (2006): Assessment of multi-span masonry bridges under in-plane seismic actions. 8NCEE, pp. 7875-7884, EERI, Oakland.

[11] Clemente P, Buffarini G, Rinaldis D (2010): Application of limit analysis to stone arch bridges. In: Baochun, C., Jiangang, W. (eds.) *ARCH'10*, 465-472. SECON-HDGK, New Art Color-Plate & Printing Co., LTD, Fujian.

[12] Clemente, P., Saitta, F. (2017): Analysis of No-Tension Material Arch Bridges with Finite Compression Strength. J. Struct. Eng., **143**(1), 04016145.

[13] Saitta F., Clemente P., Buffarini G. (2016): Analysis of Arch Bridges with Finite Compression Strength Material Under Horizontal Loadings, *Proceedings of the 8th International Conference on Arch Bridges*, Wrocław, Poland.

[14] Saitta F., Clemente P., Buffarini G., Bongiovanni G., Tripepi C. and Marzo A. (2019): Simplified model for the seismic check of masonry arch bridges with finite compression strength, *XVIII Conference of the Italian National Association of Earthquake Engineering (ANIDIS)*, Ascoli Piceno, Italy.

[15] Hughes T.G. (1995): Analysis and assessment of twin-span masonry arch bridges. Proc. Instn. Civ. Engrs Structs & Bldgs. **110**(Nov), 373-382.

[16] Brencich A. and De Francesco U. (2004): Assessment of multispan masonry arch bridges. II: Examples and Applications. J. Bridge Eng., **9**(6), 591–598.

[17] Saitta F., Clemente P., Buffarini G. and Bongiovanni G. (2019): The Mechanism Method in the Analysis of Two-Span Masonry Arch Bridges, In: Arede A and Costa C. Ed., *Proceedings of the 9th International Conference on Arch Bridges*, Porto, Portugal, 289-297, Springer.

